

DOI: 10.13208/j.electrochem.161253

Artical ID:1006-3471(2017)02-0238-07

Cite this: *J. Electrochem.* **2017**, 23(2): 238-244

Http://electrochem.xmu.edu.cn

## Electrodeposition of RuO<sub>2</sub> Layers on TiO<sub>2</sub> Nanotube Array toward CO<sub>2</sub> Electroreduction

Bei Jiang, Lina Zhang, Xianxian Qin, Wenbin Cai\*

(Shanghai Key Laboratory of Molecular Catalysis and Innovative Materials, Collaborative Innovation Center of Chemistry for Energy Materials, Department of Chemistry, Fudan University, Shanghai 200433, China)

**Abstract:** RuO<sub>2</sub>/TiO<sub>2</sub> composite materials have multitude of electrocatalytic applications including but not limited to CO<sub>2</sub> reduction reaction (CO<sub>2</sub>RR). RuO<sub>2</sub>/TiO<sub>2</sub> electrodes were previously prepared by repetitive coating and thermal decomposition (TD) of a Ru(III) precursor solution on Ti substrate. In this work, electrochemical potential cycling is applied to deposit amorphous RuO<sub>2</sub> ( $\alpha$ -RuO<sub>2</sub>) layers onto TiO<sub>2</sub> nanotube array (TNA) (RuO<sub>2</sub><sup>CV</sup>/TNA) preformed on Ti foil. SEM, GIXRD, and voltammetry are applied to characterize the structures of the resulting RuO<sub>2</sub><sup>CV</sup>/TNA. Ru loading on the RuO<sub>2</sub><sup>CV</sup>/TNA electrode is *ca.* 1/30 of that on the conventional RuO<sub>2</sub><sup>TD</sup>/TNA electrode. Although both electrodes yield similar faradaic efficiencies (FEs) for the reduction products, the RuO<sub>2</sub><sup>CV</sup>/TNA electrode displays a much higher reduction current, a more positive initial reduction potential and a better durability than the RuO<sub>2</sub><sup>TD</sup>/TNA one. In addition to higher FEs for formate and CH<sub>4</sub>, the RuO<sub>2</sub><sup>CV</sup>/TNA electrode yields the product of CO for the CO<sub>2</sub>RR in 0.1 mol·L<sup>-1</sup> KHCO<sub>3</sub>, which is not available in a PBS solution with pH 7.

**Key words:** CO<sub>2</sub> reduction; amorphous RuO<sub>2</sub>; TiO<sub>2</sub> nanotube array; electrodeposition

**CLC Number:** O646

**Document Code:** A

CO<sub>2</sub> reduction reaction (CO<sub>2</sub>RR) is receiving much attention<sup>[1-6]</sup> in considering that it may be used to convert the largest carbon resource in the atmosphere to value-added chemicals and in the meantime to reduce the greenhouse effect. CO<sub>2</sub>RR may be accomplished by means of chemical hydrogenation<sup>[1]</sup>, photochemical reduction<sup>[3,7-8]</sup> and electrochemical reduction<sup>[4]</sup>. Due to harsh conditions with chemical hydrogenation and very low efficiencies with photochemical reduction, electrochemical reduction is attractive for its mild conditions and diversities in converting CO<sub>2</sub> to CO, formate, CH<sub>3</sub>OH and other small organic molecules, especially when the electricity comes from renewable energy sources.

CO<sub>2</sub>RR on various metal catalysts were widely studied<sup>[9-12]</sup>. However, the high over-potentials and the vulnerability to cationic impurities may impede the applications of metal catalysts. In fact, very negative potentials such as -1.25 to -1.8 V vs SCE (namely large absolute over-potentials) are required to effec-

tively drive CO<sub>2</sub>RR at most metal electrodes in CO<sub>2</sub>-saturated 0.1 mol·L<sup>-1</sup> KHCO<sub>3</sub> to maintain meaningful currents<sup>[13]</sup>. The cationic impurities in solution may significantly change the activity and selectivity of the metal electrodes. To address the above concerns, metal complexes<sup>[14]</sup> and metallic oxides<sup>[15]</sup> were examined for the catalytic materials. Specifically, the conductive RuO<sub>2</sub><sup>[16-22]</sup> is expected to have smaller over-potential for CO<sub>2</sub>RR as well as hydrogen adsorption, which is essential for reducing the intermediate CO<sub>2</sub><sup>·-</sup> to formate. RuO<sub>x</sub> is unexpectedly stable even under vigorous hydrogen evolution, as a result only partial reduction to Ru ox-hydroxide occurs<sup>[22]</sup>. Along this line, additional merit of using the RuO<sub>2</sub> catalyst for CO<sub>2</sub>RR lies in its tolerance to cationic impurities in solution during CO<sub>2</sub>RR so that a much more stable reduction current may be retained.

Coating a thin layer of RuO<sub>2</sub> on TiO<sub>2</sub> substrate to form the so-called RuO<sub>2</sub>/TiO<sub>2</sub> composites<sup>[17,20,22]</sup> may further enhance electrocatalytic activity and durabili-

ty of  $\text{RuO}_2$ <sup>[17]</sup> for  $\text{CO}_2\text{RR}$ . High-temperature thermal decomposition (TD) of  $\text{RuCl}_3$  salt solution repeatedly drop-casted on Ti foil in ambient atmosphere was routinely adopted to prepare polycrystalline  $\text{RuO}_2/\text{TiO}_2$  electrodes, in which the amount of  $\text{RuO}_2$  is quite high to maintain satisfactory dispersion.

To overcome the drawbacks of the traditional TD method for preparing the  $\text{RuO}_2/\text{TiO}_2$  (denoted as  $\text{RuO}_2^{\text{TD}}/\text{TNA}$ ) electrode, in this work, the potential cycling method is extended to electrodeposit amorphous  $\text{RuO}_2$  layers onto vertically oriented  $\text{TiO}_2$  nanotube array (TNA) preformed on Ti foil (denoted as  $\text{RuO}_2^{\text{CV}}/\text{TNA}$ ) to increase the electroactive surface area while decreasing markedly the amount of  $\text{RuO}_2$  deposit. Preliminary analysis of  $\text{CO}_2\text{RR}$  on  $\text{RuO}_2^{\text{CV}}/\text{TNA}$  in pH 7 PBS and bicarbonate solutions are conducted, showing that formate,  $\text{CO}$ ,  $\text{CH}_4$  are detectable products with significant evolution of  $\text{H}_2$ .

## 1 Experimental

TNA on Ti foil was formed by means of anodization according to procedures similar to previous reports<sup>[24-28]</sup>, by using a Ti foil and a Pt sheet as the anode and the cathode, respectively. Before anodization, a mechanically polished Ti foil was first etched in the solution ( $V_{\text{H}_2\text{O}}:V_{\text{HNO}_3}:V_{\text{HF}} = 5:4:1$ ) for 1 min at room temperature. After being rinsed with copious amount of ultrapure water, the Ti foil was anodized with a voltage of 20 V in a solution containing 0.61 mL HF and 0.39 mL  $\text{CH}_3\text{COOH}$  at 30 °C for 1.5 h.

The preformed TNA was sensitized in 15  $\text{mmol} \cdot \text{L}^{-1}$   $\text{SnCl}_2 + 2 \text{mol} \cdot \text{L}^{-1}$   $\text{HCl}$  for 10 min, and then activated in 5  $\text{mmol} \cdot \text{L}^{-1}$   $\text{PdCl}_2 + 0.5 \text{mol} \cdot \text{L}^{-1}$   $\text{HCl}$  for 10 min prior to potential cycling to trigger the growth of first  $\alpha\text{-RuO}_2$  layer on TNA from -0.2 V to 1.0 V for 80 cycles at a scan rate of 50  $\text{mV} \cdot \text{s}^{-1}$  in the plating bath of 2  $\text{mmol} \cdot \text{L}^{-1}$   $\text{RuCl}_3$  and 0.10  $\text{mol} \cdot \text{L}^{-1}$   $\text{NaNO}_3$ . After that, the electrode was annealed in a muffle furnace for 2 h at 450 °C to polycrystalline  $\text{RuO}_2/\text{TNA}$  (pc- $\text{RuO}_2/\text{TNA}$ ), followed by potential cycling deposition of the second layer of  $\alpha\text{-RuO}_2$  on pc- $\text{RuO}_2/\text{TNA}$  under otherwise same conditions depicted in the above to form the  $\text{RuO}_2^{\text{CV}}/\text{TNA}$  electrode for  $\text{CO}_2\text{RR}$ . The annealing pretreatment before

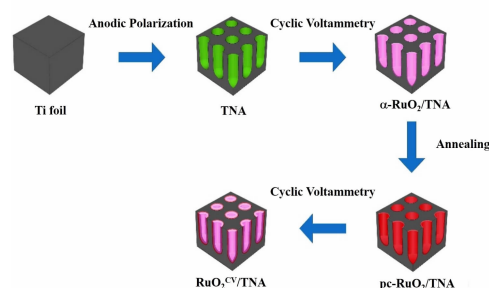


Fig. 1 Schematic illustration for preparing the  $\text{RuO}_2^{\text{CV}}/\text{TNA}$  electrode

the second electrodeposition is to increase the adhesion and stability of  $\alpha\text{-RuO}_2$  layer during  $\text{CO}_2\text{RR}$ . A schematic diagram of preparing the  $\text{RuO}_2^{\text{CV}}/\text{TNA}$  electrode is shown in Fig. 1.

For comparison,  $\text{RuO}_2^{\text{TD}}/\text{TNA}$  was prepared by thermal decomposition of alcoholic solution of 2 mg  $\text{RuCl}_3$  on TNA (2  $\text{cm}^2$ ) in a muffle furnace for 2 h at 450 °C. All electrochemical experiments were performed in a conventional three-compartment cell by using a Pt foil as the counter electrode and an SCE as the reference electrode, respectively. Linear sweep voltammograms and chronoamperometry curves were recorded in 0.2  $\text{mol} \cdot \text{L}^{-1}$   $\text{NaClO}_4$  buffered with 0.2  $\text{mol} \cdot \text{L}^{-1}$   $\text{Na}_2\text{HPO}_4\text{-NaH}_2\text{PO}_4$  (PBS, pH 7) saturated by either  $\text{N}_2$  (99.999%) or  $\text{CO}_2$  (99.999%). Potential dependent  $\text{CO}_2\text{RR}$  was conducted in  $\text{CO}_2$ -saturated 0.1  $\text{mol} \cdot \text{L}^{-1}$   $\text{KHCO}_3$  which is mostly used in literature.

The solutions were prepared with ultrapure water (Milli-Q,  $\geq 18.2 \text{ M}\Omega$ ) and AR grade reagents as received. The surface morphologies of the samples were characterized by field emission scanning electron microscopy (FE-SEM, Hitachi S-4800), and the components were analyzed by energy dispersive X-ray spectrometry (EDX, QUANTAX 400). The crystalline structures were determined by grazing incidence X-ray diffractometry (GI-XRD, New D8 advance, Bruker) at an incident angle  $\alpha_i = 0.2^\circ$ . The gas products of  $\text{CO}_2\text{RR}$  were analyzed by using the GC 2060 gas chromatography while the products dissolved in the electrolyte was analyzed by NMR (500 MHz, Bruker) and IC (Dionex DX-500).

## 2 Results and Discussion

Fig. 2A-C show the FE-SEM images for TNA before and after deposition of  $\text{RuO}_2$  layers. The  $\text{TiO}_2$  nanotubes are vertically aligned with a diameter of  $91 \pm 15$  nm and a wall thickness of  $13 \pm 3$  nm (Fig. 2A). After the first deposition of  $\alpha\text{-RuO}_2$  on TNA, the nanotube wall thickness increases to  $17 \pm 4$  nm, and it further increases to  $30 \pm 5$  nm after the second potential cycling deposition, as shown in Fig. 2B. The SEM images also indicate that  $\alpha\text{-RuO}_2$  is possibly located on the nanotube walls. In contrast, for  $\text{RuO}_2^{\text{TD}}/\text{TNA}$ , the  $\text{RuO}_2$  deposit with larger individual nanoparticles appears much thicker so that the underlying TNA is fully covered and blocked (Fig. 2 C), lowering the utilization of the  $\text{RuO}_2$  to catalyze the  $\text{CO}_2\text{RR}$ . EDX analysis reveals that the atomic ratio of Ru:Ti is 3.77:36.86 for  $\text{RuO}_2^{\text{CV}}/\text{TNA}$  and 31.11:9.77 for  $\text{RuO}_2^{\text{TD}}/\text{TNA}$ , respectively. Since the two  $\text{RuO}_2$  deposits are supported on the same TNA, the amount of Ru in the  $\text{RuO}_2^{\text{CV}}/\text{TNA}$  electrode is roughly 1/30 of that in the  $\text{RuO}_2^{\text{TD}}/\text{TNA}$  one. In other words, the elec-

trochemical deposition facilitates the control of growing ultrathin  $\text{RuO}_2$  layers over TNA, increasing significantly Ru mass utilization.

The GI-XRD (Fig. 2 D) result confirms the phase change before and after depositing and annealing  $\text{RuO}_2^{\text{CV}}/\text{TNA}$ . Before the deposition of  $\text{RuO}_2$  (Fig. 2 D (a)), only the peaks of the TNA substrate show up. After the first potential cycling deposition of  $\text{RuO}_2$  (Fig. 2 D (b)), the peaks for the TNA substrate at  $36^\circ$  and  $54^\circ$  are weakened, nevertheless no  $\text{RuO}_2$  signals can be detected, suggesting that the deposited  $\text{RuO}_2$  is amorphous<sup>[29]</sup>. After being annealed at  $450^\circ\text{C}$  for 2 h (Fig. 2 D (c)), the sample shows two peaks at  $28^\circ$  and  $35^\circ$ , featuring the transition from amorphous  $\text{RuO}_2$  structure to polycrystalline  $\text{RuO}_2$  structure. The second potential cycling deposition of  $\alpha\text{-RuO}_2$  takes place on this underlying substrate for better adhesiveness, the resulting sample is denoted as  $\text{RuO}_2^{\text{CV}}/\text{TNA}$ , which is used for following electrochemical measurements.

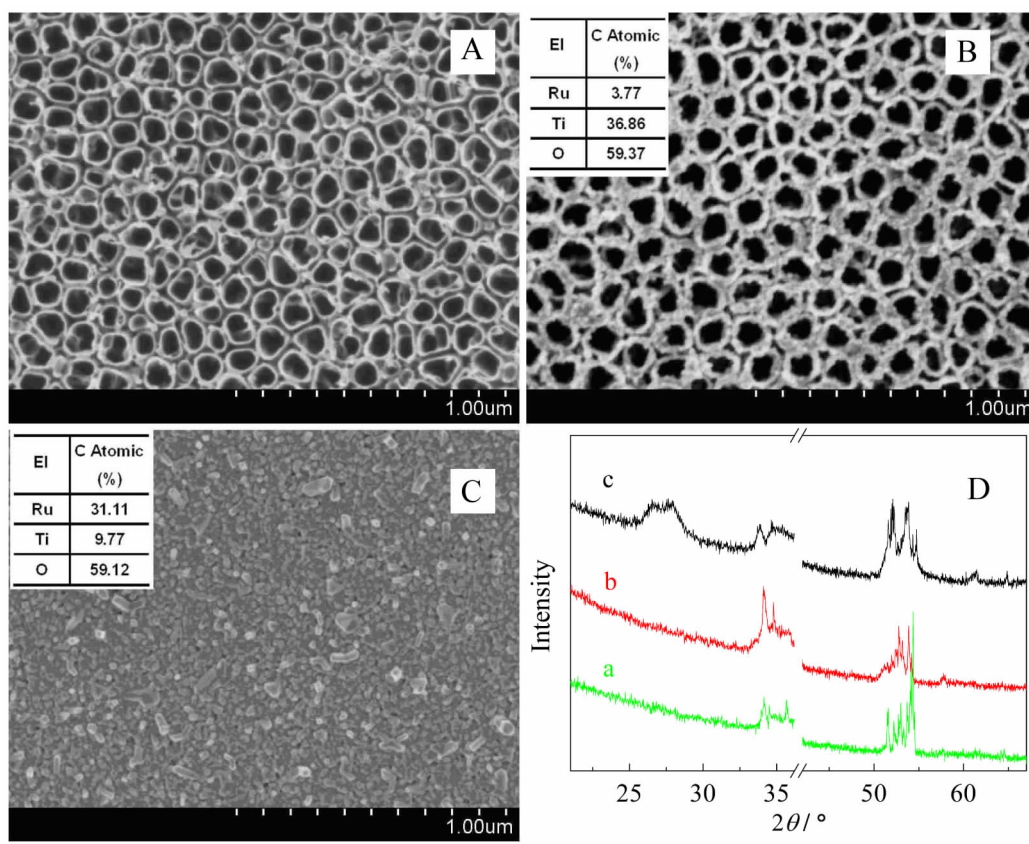


Fig. 2 FE-SEM images of as-prepared TNA (A),  $\text{RuO}_2^{\text{CV}}/\text{TNA}$  (B),  $\text{RuO}_2^{\text{TD}}/\text{TNA}$  (C), and GI-XRD (D) profiles for as-prepared TNA (a),  $\alpha\text{-RuO}_2/\text{TNA}$  (b) and  $\text{pc-RuO}_2/\text{TNA}$  (c)

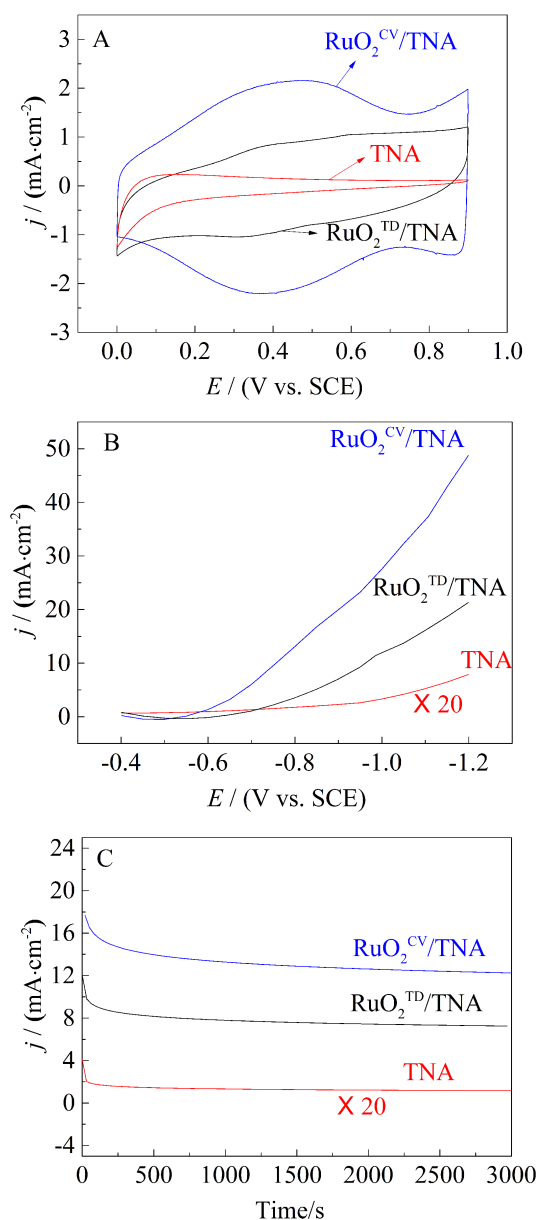


Fig.3 A. Cyclic voltammograms for  $\text{RuO}_2^{\text{CV}}/\text{TNA}$ ,  $\text{RuO}_2^{\text{TD}}/\text{TNA}$  and TNA electrodes in (A)  $0.5 \text{ mol} \cdot \text{L}^{-1} \text{H}_2\text{SO}_4$  at scan rate of  $50 \text{ mV} \cdot \text{s}^{-1}$ ; B. Linear sweep voltammograms at  $2 \text{ mV} \cdot \text{s}^{-1}$  and current vs. time plots for  $\text{CO}_2\text{RR}$  at  $-0.8 \text{ V}$  (vs. SCE) in  $\text{CO}_2$ -saturated PBS (pH 7) for  $\text{RuO}_2^{\text{CV}}/\text{TNA}$ ,  $\text{RuO}_2^{\text{TD}}/\text{TNA}$  and TNA electrodes (C).

The as-formed  $\text{RuO}_2^{\text{CV}}/\text{TNA}$  electrode was first electrochemically characterized in  $0.5 \text{ mol} \cdot \text{L}^{-1} \text{H}_2\text{SO}_4$ , showing a fish-shaped voltammogram (Fig. 3 A), indicative of the formation of an  $\alpha\text{-RuO}_2$  outer layer<sup>[29-30]</sup>, in contrast to an approximately square-shaped voltammogram for the polycrystalline  $\text{RuO}_2^{\text{TD}}/\text{TNA}$  electrode<sup>[16]</sup>. The electrocatalytic properties of the two

electrodes were simply compared by recording linear sweep voltammograms (Fig. 3B) and chronoamperometric curves (Fig. 3 C), revealing that the  $\text{RuO}_2^{\text{CV}}/\text{TNA}$  electrode is superior to the  $\text{RuO}_2^{\text{TD}}/\text{TNA}$  one in terms of electrocatalytic performance. Specifically, the  $\text{CO}_2\text{RR}$  initialized at *ca.*  $-0.6 \text{ V}$  (vs. SCE) on  $\text{RuO}_2^{\text{CV}}/\text{TNA}$ , or positively shifted by *ca.*  $0.1 \text{ V}$ , compared to that on  $\text{RuO}_2^{\text{TD}}/\text{TNA}$ , suggesting that  $\alpha\text{-RuO}_2$  may drive the  $\text{CO}_2\text{RR}$  at a smaller overpotential. Furthermore, a stabilized reduction current of *ca.*  $12 \text{ mA} \cdot \text{cm}^{-2}$  was detected on  $\text{RuO}_2^{\text{CV}}/\text{TNA}$ , which is *ca.* 1.7 times of that on  $\text{RuO}_2^{\text{TD}}/\text{TNA}$ , consistent with a larger electrochemical active surface area inherent for the  $\text{RuO}_2^{\text{CV}}/\text{TNA}$  electrode. It should be pointed out the annealing treatment after the electrodeposition of an initial layer of  $\alpha\text{-RuO}_2$  benefits the subsequent electrodeposition of a second layer of  $\alpha\text{-RuO}_2$ , leading to a larger electroactive surface area and an enhanced stability in electrocatalytic performance during  $\text{CO}_2\text{RR}$ . Table 1 lists the faradaic efficiencies (FEs) for formate,  $\text{CH}_4$  and  $\text{H}_2$  after polarizing the  $\text{RuO}_2^{\text{TD}}/\text{TNA}$  and  $\text{RuO}_2^{\text{CV}}/\text{TNA}$  electrodes at  $-0.8 \text{ V}$  in  $\text{CO}_2$ -saturated PBS solution for 452 min, respectively. Although the two electrodes yield similar FEs,  $\text{RuO}_2^{\text{CV}}/\text{TNA}$  exhibits a significantly (1.7 times) higher current density with a much lower (*ca.*  $1/30$ ) Ru mass loading than  $\text{RuO}_2^{\text{TD}}/\text{TNA}$ .

We further examined the potential dependent selectivities of  $\text{CO}_2\text{RR}$  on the  $\text{RuO}_2^{\text{CV}}/\text{TNA}$  electrode in commonly used  $\text{CO}_2$ -saturated  $0.1 \text{ mol} \cdot \text{L}^{-1} \text{KHCO}_3$  electrolyte. The solution products and the gas products were analyzed by using NMR (see Fig. 4 A) and GC (Fig. 4 B and C), respectively. The spectral data were used to quantitatively calculate FEs and partial current densities for formate,  $\text{CH}_4$  and  $\text{CO}$  as well as for  $\text{H}_2$ , at potentials varied from  $-0.8$  to  $-1.2 \text{ V}$ , see Fig. 5 A and B.

In comparison with the results listed in Tab.1, small amount of  $\text{CO}$  with FE up to 2.7% was additionally detected during  $\text{CO}_2\text{RR}$  on  $\text{RuO}_2^{\text{CV}}/\text{TNA}$  in  $0.1 \text{ mol} \cdot \text{L}^{-1} \text{KHCO}_3$  solution. It can be seen that the highest FE for formate, *ca.* 32 % occurs at  $-0.9 \text{ V}$  vs. SCE, with a highest partial reduction current of *ca.*



Tab. 1 Faradaic efficiencies for CO<sub>2</sub>RR on the RuO<sub>2</sub><sup>TD</sup>/TNA and RuO<sub>2</sub><sup>CV</sup>/TNA electrodes at -0.8 V (vs. SCE) in a PBS solution (pH 7).

Electrode	Total charge/C	Product faradaic efficiency/%			
		Formate	CH <sub>4</sub>	H <sub>2</sub>	CO
RuO <sub>2</sub> <sup>TD</sup> /TNA	31.58	30.98	1.05	32.58	Undetected
RuO <sub>2</sub> <sup>CV</sup> /TNA	45.05	29.24	1.59	34.35	Undetected

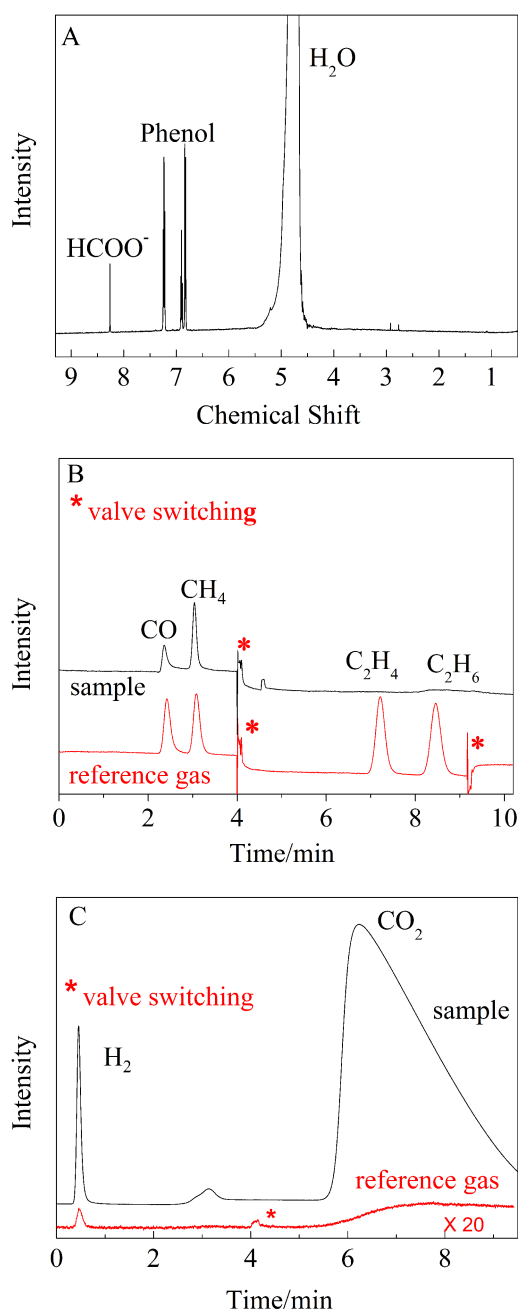


Fig. 4 A. <sup>1</sup>H NMR spectrum of the liquid products, B. GC traces from FID channels of the gas products and TCD channels of the gas products in CO<sub>2</sub>-saturated 0.1 mol·L<sup>-1</sup> KHCO<sub>3</sub> for 2 h (C).

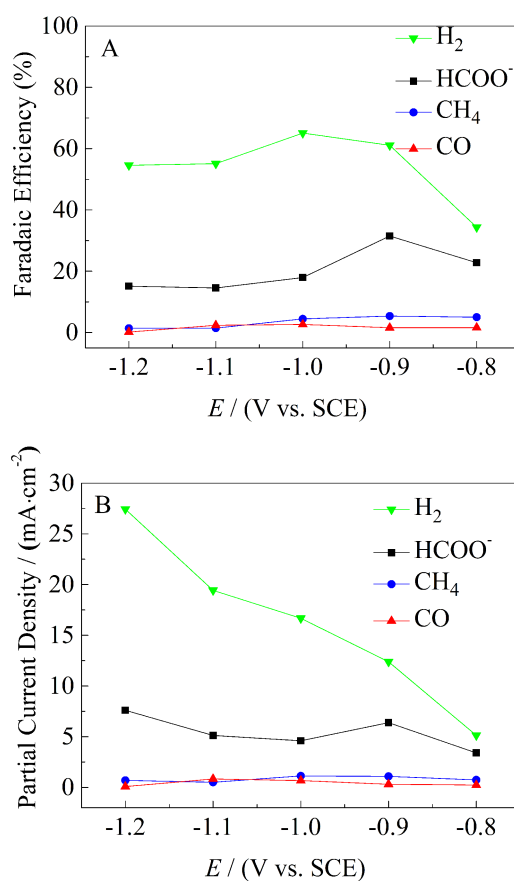


Fig. 5 Faradaic efficiencies (A) and partial current densities (B) for CO<sub>2</sub>RR on the RuO<sub>2</sub><sup>CV</sup>/TNA electrode at different potentials (vs. SCE) in CO<sub>2</sub>-saturated 0.1 mol·L<sup>-1</sup> KHCO<sub>3</sub> for 2 h

6.4 mA·cm<sup>-2</sup>. Also notably, FE for CH<sub>4</sub> varies from 1.4 % to 5.5 %, specifically it is *ca.* 5.4 % at -0.8 V and 5.5% at -0.9 V, much higher than that listed in Tab.1. It also can be seen that H<sub>2</sub> production during CO<sub>2</sub>RR contributes largely to the resulting reduction current. Further extension of the RuO<sub>2</sub><sup>CV</sup>/TNA for other electrocatalytic applications is planned.

### 3 Conclusions

In this preliminary work, a controlled deposition

of  $\alpha$ -RuO<sub>2</sub> layers on vertically oriented TNA on Ti is enabled through two-step potential cycling in a Ru(III) chloride precursor solution. The  $\alpha$ -RuO<sub>2</sub> layers are well-dispersed on the walls of the TNA without damaging the nanotube structure, and the corresponding Ru loading decreases to be *ca.* 1/30 of that for polycrystalline RuO<sub>2</sub> layers on TNA formed through thermal decomposition of a Ru(III) precursor. The RuO<sub>2</sub><sup>cv</sup>/TNA electrode displays an overall reduction current that is 1.7 times of that obtained on the RuO<sub>2</sub><sup>td</sup>/TNA one with an initial reduction potential positively shifted by 100 mV, despite that the two electrodes give the similar faradaic efficiencies for the reduction products including formate and CH<sub>4</sub> in a CO<sub>2</sub>-saturated PBS solution of pH 7. CO<sub>2</sub>RR on the RuO<sub>2</sub><sup>cv</sup>/TNA electrode in CO<sub>2</sub>-saturated 0.1 mol · L<sup>-1</sup> KHCO<sub>3</sub> produces additional CO apart from formate and CH<sub>4</sub>, showing that highest faradaic efficiencies for formate and CH<sub>4</sub> occurs at -0.9 V.

#### Acknowledgements:

This work is supported by the 973 Program (No. 2015CB932303) of MOST and NSFC (No. 21473039).

#### References:

- [1] Zhang Z F, Xie E, Li W J, et al. Hydrogenation of carbon dioxide is promoted by a task-specific ionic liquid[J]. *Angewandte Chemie International Edition*, 2008, 47(6): 1127-1129.
- [2] Barros-Antle L E, Compton R G. Reduction of carbon dioxide in 1-butyl-3-methylimidazolium acetate[J]. *Chemical Communications*, 2009, (25): 3744-3746.
- [3] Woolerton T W, Sheard S, Reisner E, et al. Efficient and clean photoreduction of CO<sub>2</sub> to CO by enzyme-modified TiO<sub>2</sub> nanoparticles using visible light[J]. *Journal of the American Chemical Society*, 2010, 132(7): 2132-2133.
- [4] Angamuthu R, Byers P, Lutz M, et al. Electrocatalytic CO<sub>2</sub> conversion to oxalate by a copper complex[J]. *Science*, 2010, 327(5963): 313-315.
- [5] Begum A, Pickup P G. Electrocatalysis of CO<sub>2</sub> reduction by ruthenium benzothiazole and bithiazole complexes[J]. *Electrochemistry Communications*, 2007, 9(10): 2525-2528.
- [6] Saha M S, Furuta T, Nishiki Y. Conversion of carbon dioxide to peroxycarbonate at boron-doped diamond electrode[J]. *Electrochemistry Communications*, 2004, 6(2): 201-204.
- [7] Liu L J, Li Ying. Understanding the reaction mechanism of photocatalytic reduction of CO<sub>2</sub> with H<sub>2</sub>O on TiO<sub>2</sub>-based photocatalysts: A review[J]. *Aerosol and Air Quality Research*, 2014, 14(2): 453-469.
- [8] Neatu S, Macia-Agullo J A, Garcia H. Solar light photocatalytic CO<sub>2</sub> reduction: General considerations and selected bench-mark photocatalysts[J]. *International Journal of Molecular Sciences*, 2014, 15(4): 5246-5262.
- [9] Reske R, Duca M, Oezaslan M, et al. Controlling catalytic selectivities during CO<sub>2</sub> electroreduction on thin Cu metal overlayers[J]. *The Journal of Physical Chemistry Letters*, 2013, 4(15): 2410-2413.
- [10] Zhang S, Kang P, Meyer T J. Nanostructured Tin catalysts for selective electrochemical reduction of carbon dioxide to formate[J]. *Journal of the American Chemical Society*, 2014, 136(5): 1734-7.
- [11] Gao D F, Wang J, Wu H H, et al. pH effect on electrocatalytic reduction of CO<sub>2</sub> over Pd and Pt nanoparticles[J]. *Electrochemistry Communications*, 2015, 55, 1-5.
- [12] Min X Q, Kanan M. Pd-catalyzed electrohydrogenation of carbon dioxide to formate: High mass activity at low overpotential and identification of the deactivation pathway[J]. *Journal of American Chemical Society*, 2015, 137(14): 4701-4708.
- [13] Hori Y. Electrochemical CO<sub>2</sub> reduction on metal electrodes[M]. *Modern Aspects of Electrochemistry*, Springer: New York, 2008, 42, 89-189.
- [14] Cheung K C, Guo P, So M H, et al. Electrocatalytic reduction of carbon dioxide by a polymeric film of rhenium tricarbonyl dipyridylamine[J]. *Journal of Organometallic Chemistry*, 2009, 694(17): 2842-2845.
- [15] Yano J, Yamasaki S. Pulse-mode electrochemical reduction of carbon dioxide using copper and copper oxide electrodes for selective ethylene formation[J]. *Journal of Applied Electrochemistry*, 2008, 38(12): 1721-1726.
- [16] Spataru N, Tokuhito K, Terashima C, et al. Electrochemical reduction of carbon dioxide at ruthenium dioxide deposited on boron-doped diamond[J]. *Journal of Applied Electrochemistry*, 2003, 33(12): 1205-1210.
- [17] Bandi A. Electrochemical reduction of carbon-dioxide on conductive metallic oxides[J]. *Journal of the Electrochemical Society*, 1990, 137(7): 2157-2160.
- [18] Chaplin R P S, Wragg A A. Effects of process conditions and electrode material on reaction pathways for carbon dioxide electroreduction with particular reference to formate formation[J]. *Journal of Applied Electrochemistry*, 2003, 33(12): 1107-1123.
- [19] Zhou S H, Eichhorn B W, Jackson G. PtCu core-shell and

- alloy nanoparticles for NO reduction; Anomalous stability and reactivity[J]. Abstracts of Papers - American Chemical Society, 2005, 230: U2145-U2145.
- [20] Bandi A, Kuhne H M. Electrochemical reduction of carbon-dioxide in water-analysis of reaction-mechanism on ruthenium-titanium-oxide[J]. Journal of the Electrochemical Society, 1992, 139(6): 1605-1610.
- [21] Qu J P, Zhang X G, Wang Y G, et al. Electrochemical reduction of CO<sub>2</sub> on RuO<sub>2</sub>/TiO<sub>2</sub> nanotubes composite modified Pt electrode[J]. Electrochimica Acta, 2005, 50 (16/17): 3576-3580.
- [22] Popic J, Avramovic M L, Vukovic N B. Reduction of carbon dioxide on ruthenium oxide and modified ruthenium oxide electrodes in 0.5 M NaHCO<sub>3</sub>[J]. Journal of Electroanalytical Chemistry, 1997, 421(1/2): 105-110.
- [23] Qin Y H, Yang H H, Lv R L, et al. TiO<sub>2</sub> nanotube arrays supported Pd nanoparticles for ethanol electrooxidation in alkaline media[J]. Electrochimica Acta, 2013, 106, 372-377.
- [24] Liu S Q, Chen A C, Coadsorption of horseradish peroxidase with thionine on TiO<sub>2</sub>: Nanotubes for biosensing[J]. Langmuir, 2005, 21(18): 8409-8413.
- [25] Yoo J, Lee K, Schmuki P. Dewetted Au films form a highly active photocatalytic system on TiO<sub>2</sub> nanotube-stumps[J]. Electrochemistry Communications, 2013, 34: 351-355.
- [26] Uddin M T, Nicolas Y, Olivier C, et al. Preparation of RuO<sub>2</sub>/TiO<sub>2</sub> mesoporous heterostructures and rationalization of their enhanced photocatalytic properties by band alignment investigations[J]. The Journal of Physical Chemistry C, 2013, 117(42): 22098-22110.
- [27] Tian M, Wu G S, Chen A C. Unique electrochemical catalytic behavior of Pt nanoparticles deposited on TiO<sub>2</sub> nanotubes[J]. ACS Catalysis, 2012, 2(3): 425-432.
- [28] Chen B, Hou J B, Lu K. Formation mechanism of TiO<sub>2</sub> nanotubes and their applications in photoelectrochemical water splitting and supercapacitors[J]. Langmuir, 2013, 29 (19): 5911-5919.
- [29] Hu C C, Huang Y H. Cyclic voltammetric deposition of hydrous ruthenium oxide for electrochemical capacitors[J]. Journal of the Electrochemical Society, 1999, 146 (7): 2465-2471.
- [30] Mo Y B, Cai W B, Dong J A, et al. *In situ* surface enhanced raman scattering of ruthenium dioxide films in acid electrolytes[J]. Electrochemical and Solid State Letters, 2001, 4(9): E37-E38.

## 在 TiO<sub>2</sub> 纳米阵列上电沉积 RuO<sub>2</sub> 用于 CO<sub>2</sub> 电还原

蒋 亭, 张莉娜, 秦先贤, 蔡文斌\*

(复旦大学化学系, 能源材料化学协同创新中心, 上海市分子催化与功能材料表面重点实验室, 上海 200433)

**摘要:** 传统上, RuO<sub>2</sub>/TiO<sub>2</sub> 复合电极制备是通过在 TiO<sub>2</sub>/Ti 基体上多次涂覆含 Ru 前驱体溶液和随后热分解(TD)来实现的. 为克服上述方法中 Ru 用量大和利用率低之不足, 本工作主要基于循环伏安法(CV)在 TiO<sub>2</sub> 纳米管阵列(TNA)上电沉积 RuO<sub>2</sub> 制备 RuO<sub>2</sub><sup>CV</sup>/TNA 复合电极. SEM、GIXRD 和 CV 结果表明, 电沉积的 RuO<sub>2</sub> 为无定型结构, 所制备电极中的 Ru 用量约为传统的 RuO<sub>2</sub><sup>TD</sup>/TNA 电极中 Ru 用量的 1/30. 尽管两电极催化 CO<sub>2</sub> 还原产物的法拉第效率接近, 但是 RuO<sub>2</sub><sup>CV</sup>/TNA 电极比 RuO<sub>2</sub><sup>TD</sup>/TNA 电极展示了更高的还原电流, 较正的初始还原电位和更好的稳定性. 与磷酸盐缓冲溶液中电还原 CO<sub>2</sub> 相比, RuO<sub>2</sub><sup>CV</sup>/TNA 电极在 0.1 mol·L<sup>-1</sup> KHCO<sub>3</sub> 中电还原 CO<sub>2</sub> 除生成更高法拉第效率的甲酸根和甲烷外, 还检测到 CO 的生成.

**关键词:** CO<sub>2</sub> 还原; 无定型 RuO<sub>2</sub>; TiO<sub>2</sub> 纳米阵列; 电沉积